THE JOURNAL OF PHYSICAL CHEMISTRY C

Article

pubs.acs.org/JPCC

Pressure-Collapsed Amorphous $Mg(BH_4)_2$: An Ultradense Complex Hydride Showing a Reversible Transition to the Porous Framework

Voraksmy Ban,[†] Alexei V. Soloninin,[‡] Alexander V. Skripov,*[,‡] Joke Hadermann,[§] Artem Abakumov,[§] and Yaroslav Filinchuk*[,†]

[†]Institute of Condensed Matter and Nanosciences, Université Catholique de Louvain, Place L. Pasteur 1, 1348 Louvain-la-Neuve, Belgium

[‡]Institute of Metal Physics, Ural Division of the Russian Academy of Sciences, S. Kovalevskoi 18, Ekaterinburg 620990, Russia

[§]EMAT, University of Antwerp, Groenenborgerlaan 171, 2020 Antwerp, Belgium

Supporting Information

ABSTRACT: Hydrogen-storage properties of complex hydrides depend of their form, such as a polymorphic form or an eutectic mixture. This Paper reports on an easy and reproducible way to synthesize a new stable form of magnesium borohydride by pressure-induced collapse of the porous γ-$Mg(BH_4)_2$. This amorphous complex hydride was investigated by temperature-programmed synchrotron X-ray diffraction (SXRD), transmission electron microscopy (TEM), thermogravimetric analysis, differential scanning calorimetry analysis, and Raman spectroscopy, and the dynamics of the BH_4^- reorientation was studied by spin−lattice relaxation NMR spectroscopy. No long-range order is observed in the lattice region by Raman spectroscopy, while the internal vibration modes of the BH_4^- groups are the same as in the crystalline state. A hump at 4.9 Å in the SXRD pattern suggests the presence of nearly linear Mg−BH_4−Mg fragments constituting all the known crystalline polymorphs of $Mg(BH_4)_2$, which are essentially frameworks built of tetrahedral Mg nodes and linear BH_4 linkers. TEM shows that the pressure-collapsed phase is amorphous down to the nanoscale, but surprisingly, SXRD reveals a transition at ∼90 °C from the dense amorphous state (density of 0.98 g/cm^3) back to the porous γ phase having only 0.55 g/cm^3 crystal density. The crystallization is slightly exothermic, with the enthalpy of −4.3 kJ/mol. The volumetric hydrogen density of the amorphous form is 145 g/L, one of the highest among hydrides. Remarkably, this form of $Mg(BH_4)_2$ has different reactivity compared to the crystalline forms. The parameters of the reorientational motion of BH_4 groups in the amorphous $Mg(BH_4)_2$ found from NMR measurements differ significantly from those in the known crystalline forms. The behavior of the nuclear spin−lattice relaxation rates can be described in terms of a Gaussian distribution of the activation energies centered on 234 ± 9 meV with the dispersion of 100 ± 10 meV.

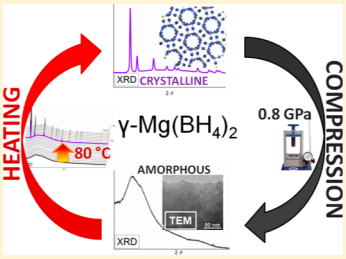

INTRODUCTION

High gravimetric and volumetric hydrogen densities are the main requirements for potential hydrogen-storage materials. Thus, complex hydrides and especially light metal borohydrides are extensively studied for this purpose.[1,2] Magnesium borohydride and its multiple polymorphs are very promising candidates, given its hydrogen desorption reversibility[3] and formation of reversible reactive hydride composites.[4] Magnesium borohydride exists in a form of various polymorphs,[5−10] having framework structures and very different densities. In particular, the recently discovered porous form of $Mg(BH_4)_2$ having 14.9 wt % covalently bound hydrogen can store an additional 3 wt % of physisorbed molecular H_2 at low temperatures.[5] The form of the solid hydride can be determinative for the decomposition reaction pathway and thus for the hydrogen desorption reversibility. For instance, many borohydrides yield upon heating stable $[B_{12}H_{12}]^{2-}$ species that decrease their hydrogen release potential and prevent their reversibility; see a review[11]. This mechanism is one of the obstacles for $Mg(BH_4)_2$ rehydrogenation.[12] However, nanoconfined eutectic $LiBH_4$−$Mg(BH_4)_2$, reported to be amorphous, revealed a different behavior upon a thermal decomposition, that is, suppressed formation of $[B_{12}H_{12}]^{2-}$ species suggesting a possible reversibility of the dehydrogenation.[13] Generally, X-ray diffraction (XRD) is a powerful tool to characterize complex hydrides and products of their dehydrogenation,[14] but it is helpless for amorphous substances. This is one of the main reasons why amorphous phases were often not recognized in the mixtures and thus not always considered in the reaction mechanisms. Amorphous $Mg(BH_4)_2$ has been obtained in a few experiments. For example, an extensive high-energy ball milling of a crystalline form results in a partial or even a total amorphization of $Mg(BH_4)_2$.[5,15] Another example is the hydrogenation of MgB_2 leading to the formation of $Mg(BH_4)_2$ but in an amorphous form.[16] Also, the compression of the porous γ-$Mg(BH_4)_2$ in a diamond anvil cell leads to a highly dense δ-$Mg(BH_4)_2$ phase, occurring via an intermediate formation of a fully amorphous sample.[5]

Received: July 21, 2014
Revised: September 11, 2014
Published: September 11, 2014

In this work, we show that the pressure-collapsed amorphous form of $Mg(BH_4)_2$ is stable under ambient conditions and thus can be obtained in bulk quantities using standard stainless steel dies. Here, we present the first detailed study of an amorphous complex hydride, which includes its synthesis in bulk, variable temperature synchrotron XRD study, specific density measurement, thermogravimetric analysis (TGA) and differential scanning calorimetry analysis (DSC), study by transmission electron microscopy (TEM) and Raman spectroscopy, as well as NMR study of the rotational motion of the BH_4 groups. All these techniques show distinctly different properties of the amorphous form compared to the numerous crystalline $Mg(BH_4)_2$ polymorphs.[5−10] The pressure-collapsed amorphous magnesium borohydride turns out to have one of the highest volumetric hydrogen densities and can thus be used as a component in efficient reactive hydride composites, promising materials for hydrogen storage. We will not focus on a possible polyamorphism of $Mg(BH_4)_2$, that is, possibly different amorphous phases. However, precautions were taken to prepare the pure pressure-collapsed amorphous magnesium borohydride by compressing the highly crystalline porous γ-$Mg(BH_4)_2$.

EXPERIMENTAL METHODS

We have recently found that, on a long-term storage at room temperature, the porous γ-$Mg(BH_4)_2$ slowly amorphisizes. Therefore, fresh highly crystalline γ-$Mg(BH_4)_2$ was used in the synthesis of the pure pressure-collapsed amorphous phase. The porous γ-$Mg(BH_4)_2$ was obtained by a wet chemical method from dibutylmagnesium and a dimethylsulfide (DMS) complex of borane, followed by vacuum removal of DMS from $Mg(BH_4)_2 \cdot {}^1/_2 DMS$.[5]

The fresh γ-$Mg(BH_4)_2$ was loaded into a 4 mm diameter pellet die inside an argon glovebox and slightly prepressed. The whole set is then wrapped with parafilm to avoid the contact with air during the transfer between the glovebox and the press. Then, outside the glovebox, the pellet was made by compressing two times the γ-$Mg(BH_4)_2$ at 0.8 GPa. The whole compression operation lasts 5−6 min. The die with the sample was then put back inside the glovebox for the extraction of the pellet.

In situ synchrotron XRD (SXRD) powder data were collected at the Swiss−Norwegian beamline BM1A at the European Synchrotron Radiation Facility (ESRF, Grenoble, France) using PILATUS 2 M pixel detector and radiation with 0.68884 Å wavelength. The samples were enclosed under argon into 0.5 mm diameter thin-walled glass capillaries. The temperature program was controlled by an Oxford Cryostream 700+ or a Cyberstar hot gas blower at a rate of 5 °C per minute from room temperature to 320 °C. The two-dimensional images were azimuthally integrated using Fit2D program and LaB_6 standard data.

TEM images and energy-dispersive X-ray (EDX) spectra were acquired using a Tecnai G2 microscope operating at 200 kV. The sample of pressure-collapsed $Mg(BH_4)_2$ was crushed using an agate mortar and pestle and dispersed in anhydrous hexane, and a few drops of this dispersion were deposited on a copper grid with a holey carbon film. This procedure was performed in an argon glovebox. The sample was loaded inside this glovebox into a transfer holder and transported to a microscope column avoiding contact with air at all times. High-angle annular dark field (HAADF) scanning transmission electron microscopy (STEM) images were taken with very short exposure times to avoid beam damage induced by a prolonged probe scanning.

Thermal analysis data were independently collected using TGA/sDTA 851e and DSC 821 Mettler instruments. TGA and DSC measurements were performed on the pressure-collapsed amorphous $Mg(BH_4)_2$ and on a fresh γ-$Mg(BH_4)_2$ from the same batch as used in the compression experiment. The samples for the TGA and DSC analysis were loaded in an argon glovebox into alumina crucibles and covered with a cap or sealed into a small aluminum pan, respectively. Both types of experiments were done under nitrogen flow, with 5 °C/min heating from room temperature to 500 °C. A number of experiments was done on samples from different synthesis runs until a consistent and reproducible picture was obtained.

The vibrational spectra of the crystalline γ-$Mg(BH_4)_2$ and the amorphous $Mg(BH_4)_2$ were collected at room temperature with a Bruker RFS 100/S FT-Raman spectrometer (I = 200 mW) in the 100−4000 cm^{-1} range using a diode-pumped Nd:YAG laser operated at 1064 nm excitation. The samples were loaded into glass capillaries in an argon glovebox and sealed with vacuum grease to prevent any contact with air.

NMR measurements were performed on a pulse spectrometer with quadrature phase detection at the frequencies $\omega/2\pi$ = 14, 28, and 90 MHz for ^1H and 14 and 28 MHz for ^{11}B. For NMR experiments, the sample was sealed in a NMR glass tube under ∼500 mbar of nitrogen gas. The magnetic field was provided by a 2.1 T iron-core Bruker magnet. A home-built multinuclear continuous-wave NMR magnetometer working in the range 0.32−2.15 T was used for field stabilization. For rf pulse generation, we used a home-built computer-controlled pulse programmer, the PTS frequency synthesizer (Programmed Test Sources, Inc.), and a 1 kW Kalmus wideband pulse amplifier. Typical values of the $\pi/2$ pulse length were 2−3 μs for both ^1H and ^{11}B. A probehead with the sample was placed into an Oxford Instruments CF1200 continuous-flow cryostat using helium or nitrogen as a cooling agent. The sample temperature in the range 10−298 K, monitored by a chromel-(Au−Fe) thermocouple, was stable to ±0.1 K. The nuclear spin−lattice relaxation rates were measured using the saturation−recovery method. NMR spectra were recorded by Fourier transforming the solid echo signals (pulse sequence $\pi/2_x - t - \pi/2_y$).

RESULTS AND DISCUSSION

The size and mass of the dense pellet of the amorphous $Mg(BH_4)_2$ were carefully measured, yielding 0.976 ± 0.02 g/cm^3 density, very close to the 0.987 g/cm^3 diffraction density found for the crystalline high-pressure δ phase.[5] The pellet does not gain any weight on air, indicating this form is much less sensitive to humidity than the fluffy powder of crystalline α-, β- and γ-$Mg(BH_4)_2$, which should be manipulated under an inert atmosphere. The volumetric hydrogen density of the amorphous form is 145 g/L, one of the highest among hydrides.

The XRD pattern of the pressure-collapsed amorphous $Mg(BH_4)_2$, shown as the lower trace in Figure 1, reveals at room temperature an amorphous hump at ∼4.9 Å, consistent with a broad halo at 4.78−4.30 Å observed within 0.4−2.0 GPa pressure in diamond anvil cells.[5] Diffraction-amorphous $Mg(BH_4)_2$ synthesized by high-energy ball milling of MgB_2 in H_2 atmosphere shows the same broad peak with d spacing of 4.9 Å at ambient conditions,[16] while an amorphous $Mg(BH_4)_2$ synthesized by high-energy ball milling of γ-$Mg(BH_4)_2$ under

dx.doi.org/10.1021/jp507286m | J. Phys. Chem. C 2014, 118, 23402−23408

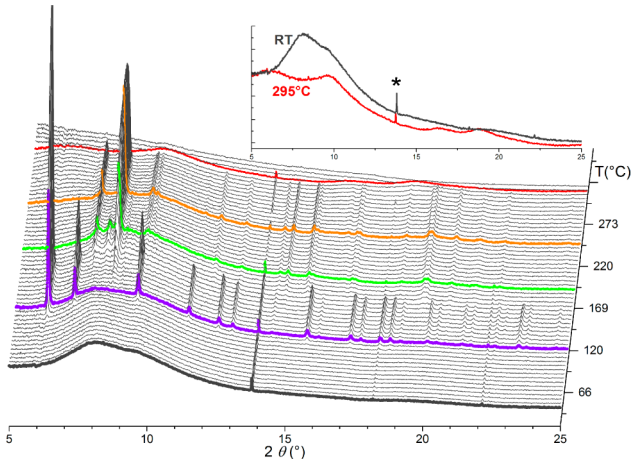

Figure 1. In situ SXRD powder data on the amorphous $Mg(BH_4)_2$ sample measured under protective Ar atmosphere from 25 to 300 °C, λ = 0.68884 Å. The amorphous $Mg(BH_4)_2$ phase (gray line) transforms upon heating into the γ phase (purple line), which in turn transforms into the β'+ε phases (green line), the β' phase (orange line), and at last, to the amorphous decomposition products (red line). The * symbol in the inset marks the iron peak contamination from the die set.

argon shows a hump at lower d spacing of 4.7 Å (see Chapter 19 in the Supporting Information to ref 5). No peaks from any of the $Mg(BH_4)_2$ polymorphs were observed. The other hump at 4.1 Å is due to the scattering from the quartz capillary where the sample was enclosed, as confirmed by a blank measurement. The halo at 4.9 Å may correspond to the Mg···Mg distance observed in the nearly linear Mg−BH_4−Mg fragments constituting the porous γ and the denser δ polymorphs of $Mg(BH_4)_2$, which are essentially frameworks built of tetrahedral Mg nodes and linear BH_4 linkers.[5] This halo seems to indicate that the amorphous phase has locally similar structure, containing the stable nearly linear Mg−BH_4−Mg fragment, but further studies as a pair distribution function analysis would give a clear answer.

Upon heating, the amorphous phase transforms into the porous γ phase between 90 and 135 °C. This is a surprising observation, since the density of $Mg(BH_4)_2$ decreases by almost two times on this transition, from 0.98 to 0.55 g/cm^3, without going through the denser α phase (0.78 g/cm^3). The β' phase (β phase with no odd hkl peaks) appears above 155 °C with the ε phase, both recently mentioned in refs 8−10 and 17, when the diffraction peaks of the porous phase disappear. Between 210 and 260 °C, only the β' phase remains. At higher temperatures, a decomposition occurs at 270 °C with the decrease of the intensity of the β' phase diffraction peaks and the appearance of the amorphous humps at d = 6.5, 2.45, and 2.12 Å at 295 °C, in agreement with data published earlier.[9,10] The amorphous humps found for the pressure-induced amorphous phase at room temperature, d = 4.9, 2.02 Å, are drastically different from the humps identified for the high-temperature amorphous phase. No correlation can be made between these two distinct amorphous phases. The loss of crystallinity of these two amorphous states are induced by different factors: the amorphous phase at room temperature corresponding to the loss of the local structure due to the compression of γ-$Mg(BH_4)_2$ and the high-temperature amorphous phase corresponding more likely to the decomposition of $Mg(BH_4)_2$.

The fact of the transformation of the dense amorphous phase into the porous γ phase on heating is unexpected as the porous phase was earlier obtained only by templating magnesium borohydride with small solvent molecules and removing the latter by vacuum. Also, the porous crystalline phase does not form from any other crystalline polymorph known so far,[8] under any temperature and pressure conditions. Its formation from the amorphous phase thus questions whether the pressure-collapsed phase is truly amorphous or it may contain ordered nanodomains with the porous structure serving as crystallization seeds. This hypothesis was verified by TEM, showing that the pressure-collapsed phase is truly amorphous, down to the nanoscale (see below). The ability to transform to the porous γ phase may be an intrinsic property of the pressure-collapsed amorphous phase, in case a polyamorphism indeed occurs in $Mg(BH_4)_2$.

EDX spectra taken from 10 random particles are all similar, as shown in Figure 2a. On the spectra, not only the peaks from

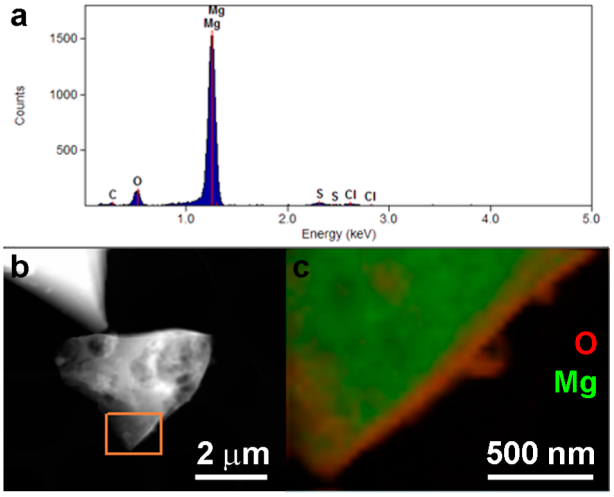

Figure 2. (a) EDX spectrum of the amorphous $Mg(BH_4)_2$ particle; (b) HAADF-STEM image and (c) with a region selected for the EDX compositional mapping and the mixed EDX map of the Mg−K edge and O−K edge.

Mg are present (B and H are too light to detect) but also a noticeable oxygen peak, as well as small peaks indicating traces of S and Cl. The carbon peak is due to the support used for the crystals during the TEM experiment, and the sulfur peaks are from the remaining solvent. The intensity ratio of the Mg K and O K peaks varies significantly depending on the selected area indicating inhomogeneity of the oxygen distribution. Figure 2b, c and Figure S1 (Supporting Information) show HAADF-STEM images with accompanying EDX Mg and O maps of several particles. The EDX maps clearly reveal that the oxygen signal originates from the surface layer with the thickness of 50−100 nm, surrounding the particles. The oxidized amorphous surface layer might be a reason for the low sensitivity of amorphous $Mg(BH_4)_2$ to oxygen and moisture as it effectively blocks further diffusion of these species toward the interior of the particle.

Figure 3 shows a low-magnification TEM image of the particles and a high-resolution (HR) TEM image of a particle taken at low dose condition. The HR-TEM image of the particles confirms the amorphous state of the pressure-collapsed $Mg(BH_4)_2$ and that no crystallinity was detected, down to the nanoscale.

dx.doi.org/10.1021/jp507286m | J. Phys. Chem. C 2014, 118, 23402−23408

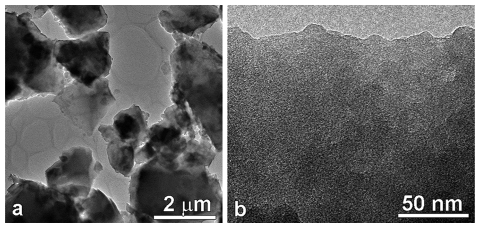

Figure 3. (a) Low-magnification TEM image and (b) HR-TEM image of a particle, showing clearly the amorphous character.

The evolution of this particle under electron beam irradiation, shown step by step in Figure S2 (Supporting Information), demonstrates that the particles consist of an amorphous $Mg(BH_4)_2$ core, which gradually decomposes at increasing electron irradiation dose. The core is surrounded by an amorphous surface layer (noticeable as a lighter edge), which is not sensitive toward the electron beam, being the oxidized surface layer revealed by the EDX analysis. Thus, the sample consists of fully amorphous $Mg(BH_4)_2$ particles surrounded by an oxygen-containing surface layer.

Thermal analysis experiments (Figure 4) of the pressure-collapsed amorphous $Mg(BH_4)_2$ and the porous γ-$Mg(BH_4)_2$

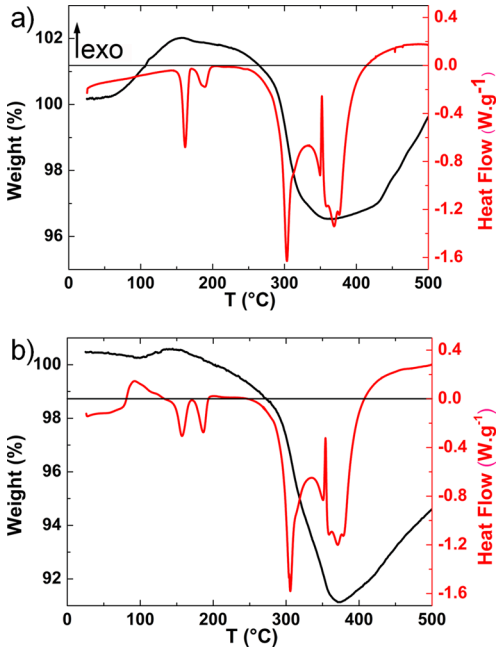

Figure 4. Combined mass loss (in black) and heat flow (in red) curves measured with independent TGA and DSC experiments for (a) the porous γ-$Mg(BH_4)_2$ and (b) the pressure-collapsed amorphous $Mg(BH_4)_2$.

were done on samples from different synthesis runs until a consistent and reproducible picture was obtained. The interpretation of the TGA curves above 300 °C is delicate as there is a competition between the weight loss due to their decompositions and the weight gain from the magnesium nitridation.[18]

As consistent with the diffraction data, the decomposition profiles of both samples are very similar at higher temperatures: the TGA profiles show a clear weight loss from 280 °C, and the DSC profiles display the same endothermic peaks corresponding to the transformations between different crystalline polymorphs and finally due to the decomposition. However, the thermal decomposition profile of the amorphous phase exhibits an additional broad exothermic peak centered at 92 °C and clearly associated with the crystallization of the amorphous phase into the γ-$Mg(BH_4)_2$. The temperature of crystallization coincides perfectly with the appearance of the γ-$Mg(BH_4)_2$ observed with in situ SXRD powder data. The enthalpy of the crystallization is estimated at −4.3 kJ/mol, which is comparable to values published for other inorganic salts, such as $CaCO_3$ (−14.3 kJ/mol[19]).

Considering that little information can be drawn on the structure of the amorphous $Mg(BH_4)_2$ by diffraction methods, we used Raman and NMR spectroscopy to identify the local structure and probe the dynamics of this new phase. Figure 5

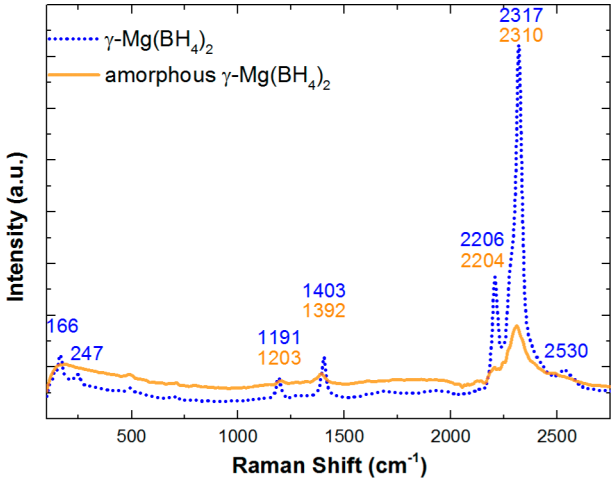

Figure 5. Raman spectra of the crystalline γ-$Mg(BH_4)_2$ and of the pressure-collapsed amorphous $Mg(BH_4)_2$ at room temperature. The shifts are indicated in different colors for the different phases.

shows the Raman spectrum of the amorphous $Mg(BH_4)_2$. The characteristic absorption bands of the crystalline $Mg(BH_4)_2$ are also present in the Raman spectrum of the amorphous phase: the B−H stretching modes around 2300 cm^{-1} and the BH_4 bending modes between 1000 and 1400 cm^{-1}. However, the bands are broader and less intense than for the crystalline γ phase (the two spectra in Figure 5 were taken in the same conditions and with the same exposure time). The lower frequency of the 1392 cm^{-1} mode, assigned to the ν_2 bending, can be correlated with a weaker interaction of the BH_4^- anion bidentately coordinated to the Mg^{2+} ions in the amorphous phase.[20] No bands are observed in the lattice region for the amorphous phase, except those between 400 and 700 cm^{-1} from the vacuum grease used for the measurement. The broader and weaker Raman bands for the pressure-collapsed amorphous phase contrast somewhat narrower and more intense peaks of the amorphous $Mg(BH_4)_2$ obtained by high-energy ball milling (see Figures S18 and S19 in ref 5). However, only small differences for the Raman shifts between the amorphous and crystalline $Mg(BH_4)_2$, suggest that their local structures are identical.

NMR measurements have been performed below room temperature in order to prevent any phase changes. Figure 6 shows the behavior of the proton spin−lattice relaxation rate R_1^H measured at three resonance frequencies as a function of the inverse temperature. It can be seen that $R_1^H(T)$ exhibits the frequency-dependent peak, which is typical of the relaxation

dx.doi.org/10.1021/jp507286m | J. Phys. Chem. C 2014, 118, 23402−23408

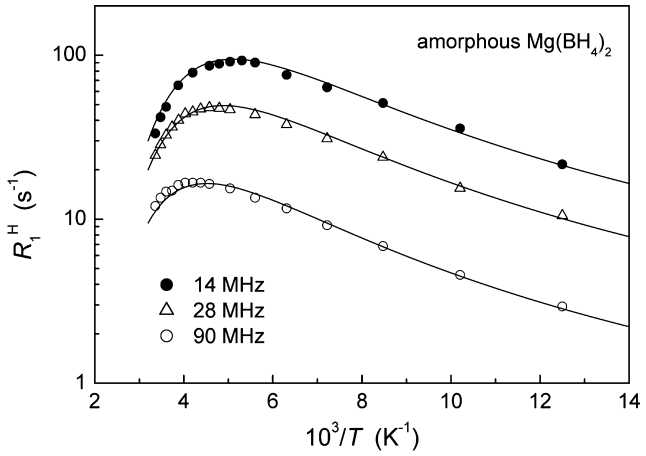

Figure 6. Proton spin–lattice relaxation rates measured at 14, 28, and 90 MHz for the amorphous $Mg(BH_4)_2$ as functions of the inverse temperature. The solid lines show the simultaneous fit of the model with a Gaussian distribution of the activation energies to the data.

mechanism due to the nuclear dipole–dipole interaction modulated by atomic motion.[21] For this mechanism, the $R_1^H(T)$ maximum is expected to occur at the temperature at which the H jump rate τ^{-1} becomes nearly equal to the resonance frequency ω. Thus, the position of the $R_1^H(T)$ peak may serve as an indicator of the H mobility in different systems. For the systems with higher H jump rates, the $R_1^H(T)$ peak should occur at lower temperatures. As for the crystalline phases of $Mg(BH_4)_2$,[17,22−24] the $R_1^H(T)$ peak for the amorphous $Mg(BH_4)_2$ originates from reorientations of the BH_4 groups. This is supported by the behavior of the ^{1}H NMR line width, to be discussed below. It should be noted that the position of the $R_1^H(T)$ peak for the amorphous $Mg(BH_4)_2$ differs significantly from the corresponding positions for all the crystalline $Mg(BH_4)_2$ phases studied so far. In fact, for the amorphous $Mg(BH_4)_2$, the $R_1^H(T)$ maximum at $\omega/2\pi$ = 14 MHz is observed near 190 K, while for the crystalline α, β, and γ phases, the $R_1^H(T)$ maxima at the same frequency occur near 290,[24] 120,[22] and 270 K,[22] respectively. This means that the amorphous phase of $Mg(BH_4)_2$ exhibits its own distinct dynamics of BH_4 reorientations.

According to the standard theory[21] of nuclear spin–lattice relaxation due to atomic motion with a single jump rate τ^{-1}, in the limit of slow motion ($\omega\tau \gg 1$), R_1^H should be proportional to $\omega^{-2}\,\tau^{-1}$, and in the limit of fast motion ($\omega\tau \ll 1$), R_1^H should be proportional to τ, being frequency independent. If the temperature dependence of the jump rate is governed by the Arrhenius law, $\tau^{-1} = \tau_0^{-1}\exp(-E_a/k_BT)$, a plot of ln R_1^H versus T^{-1} should be linear in the limits of both slow and fast motions with the slopes of $-E_a/k_B$ and E_a/k_B, respectively. As can be seen from Figure 6, the experimental $R_1^H(T)$ data for the amorphous $Mg(BH_4)_2$ exhibit significant deviations from this simple picture. First, the high-temperature slope of the $R_1^H(T)$ peak appears to be steeper than the low-temperature one. Second, the frequency dependence of R_1^H at the low-temperature slope is much weaker than the expected ω^{-2} dependence. These features are consistent with the presence of a broad distribution of H jump rates,[25] which can be expected for the amorphous system. The simplest model for parametrization of the jump rate distribution is based on a Gaussian distribution of E_a values.[25] The parameters of this model are the pre-exponential factor τ_0, the average activation energy $\bar{E}_a$, and the width of the distribution (dispersion) ΔE_a. These motional parameters (and the amplitude parameter characterizing the strength of dipole–dipole interactions) have been varied to find the best fit to the $R_1^H(T)$ data at the three resonance frequencies simultaneously. The results of the simultaneous fit of the model with a Gaussian distribution of the activation energies to the data are shown by the solid curves in Figure 6. The corresponding values of the motional fit parameters are $\tau_0 = (1.1 \pm 0.4) \times 10^{-15}$ s, $\bar{E}_a = 234 \pm 9$ meV, and $\Delta E_a = 100 \pm 10$ meV. The activation energies for BH_4 reorientations, as derived from our proton NMR measurements in the amorphous and crystalline phases of $Mg(BH_4)_2$ are compared in Table 1. The three values of the activation energy for α-$Mg(BH_4)_2$ correspond to three coexisting reorientational processes in this phase.[24] As can be seen from Table 1, the average activation energy for the amorphous $Mg(BH_4)_2$ differs significantly from those for the crystalline $Mg(BH_4)_2$ phases. The value of the distribution width ΔE_a for the amorphous $Mg(BH_4)_2$ is the largest among all the studied $Mg(BH_4)_2$ phases.

Table 1. Activation Energies for BH_4 Reorientations in Different Phases of $Mg(BH_4)_2$, As Derived from the Proton NMR Experiments[a]

compd	activation energy E_a or $\bar{E}_a$ (meV)	dispersion of the E_a distribution (meV)	ref
α-$Mg(BH_4)_2$	116 (6), 298 (12), 362 (5)	10 (4)	24
β-$Mg(BH_4)_2$	138 (5)	36 (3)	22
γ-$Mg(BH_4)_2$	276 (5)	19 (4)	22
amorphous $Mg(BH_4)_2$	234 (9)	100 (10)	this work

[a]Uncertainties in the last digit are given in parentheses.

Figure 7 shows the temperature dependence of the width (full width at half-maximum, $\Delta\nu$) of the ^{1}H NMR spectrum measured at 28 MHz for the amorphous phase of $Mg(BH_4)_2$. The observed significant line narrowing near 70 K indicates the excitation of the H jump motion on the frequency scale of the order of 10^5 s^{-1}. Above the temperature of ~120 K, the proton line width stops to decrease, being nearly constant up to the highest temperature of our measurements. The substantial plateau value of $\Delta\nu$ (~24 kHz) indicates that the motion responsible for the observed line narrowing is indeed localized

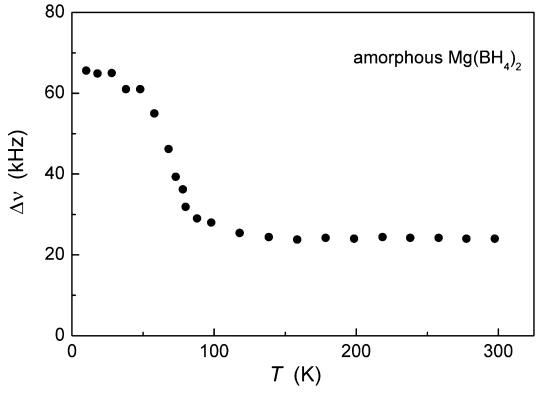

Figure 7. Temperature dependence of the width (full width at half-maximum) of the proton NMR spectrum measured at 28 MHz for the amorphous $Mg(BH_4)_2$.

dx.doi.org/10.1021/jp507286m | J. Phys. Chem. C 2014, 118, 23402−23408

because such a motion leads to only partial averaging of dipole−dipole interactions between nuclear spins. Similar behavior of the proton NMR line width was observed for the crystalline phases of $Mg(BH_4)_2$.[22,24]

The recovery of the ^{11}B nuclear magnetization for the amorphous $Mg(BH_4)_2$ is found to deviate from the single-exponential behavior. In the studied temperature range, the ^{11}B recovery curves can be reasonably approximated by a sum of two exponential functions. The two-exponential ^{11}B relaxation was also observed in some crystalline borohydrides;[23,26] such a behavior may be related[21] to the nonzero electric quadrupole moment of this nucleus. In our case, the two-exponential recovery is dominated by the faster component R_{1F}^B. The temperature dependences of the faster components of the ^{11}B spin−lattice relaxation rate at two resonance frequencies are shown in Figure 8. The considerable scatter of the data points in this figure can be attributed to certain instability of the two-exponential description of the recovery curves.

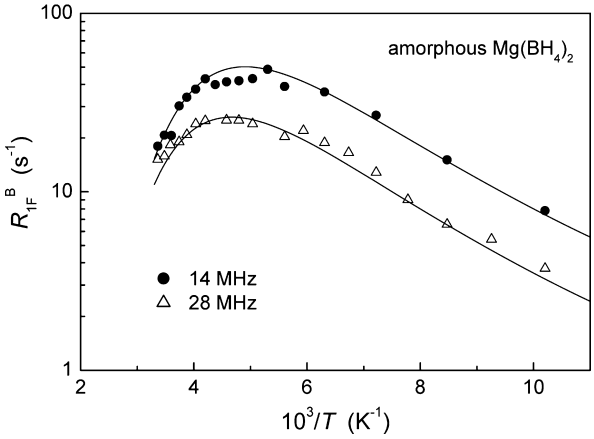

Figure 8. Fast components of the ^{11}B spin−lattice relaxation rates measured at 14 and 28 MHz for the amorphous $Mg(BH_4)_2$ as functions of the inverse temperature. The solid lines show the simultaneous fit of the model with a Gaussian distribution of the activation energies to the data.

However, the $R_{1F}^B(T)$ maximum is observed at nearly the same temperature as the corresponding $R_1^H(T)$ maximum, and the general features of the behavior of R_{1F}^B are similar to those of R_1^H (see Figure 6). Therefore, for parametrization of $R_{1F}^B(T)$, we have used the same model with a Gaussian distribution of the activation energies. The solid curves in Figure 8 show the simultaneous fit of this model to the $R_{1F}^B(T)$ data at two resonance frequencies. The corresponding motional fit parameters are $\tau_0 = (4 \pm 1) \times 10^{-15}$ s, $\bar{E}_a = 233 \pm 12$ meV, and $\Delta E_a = 70 \pm 10$ meV. The value of the average activation energy obtained from the ^{11}B relaxation data appears to be very close to that derived from the proton relaxation data. It should be noted that our present NMR results for the amorphous $Mg(BH_4)_2$ support the idea[22] that the parameters of the reorientational motion are very sensitive to subtle details of local environment of BH_4 groups.

CONCLUSIONS

The amorphous $Mg(BH_4)_2$ obtained by pressure collapse of the porous γ-$Mg(BH_4)_2$ is a distinct and a stable form of magnesium borohydride, with one of the highest volumetric hydrogen densities of 145 g/L, close to that of the high-pressure δ-$Mg(BH_4)_2$.[5] This substance is amorphous down to the nanoscale, while it is locally built of the same Mg−BH_4−Mg fragments as all the known crystalline polymorphs of $Mg(BH_4)_2$. Thus, the pressure-induced amorphization of the framework built of tetrahedral Mg nodes and linear BH_4 linkers, resembles a collapse observed for the porous metal−organic frameworks (MOFs) at high pressures.[27] However, the pressure-amorphisized MOFs are not capable of transforming under increased pressure to crystalline dense frameworks[5] or back-converting under increased temperatures to the porous framework, like we describe in this work.

The dynamics of the reorientational motion of the BH_4 groups in the amorphous $Mg(BH_4)_2$ differs significantly from those in the known crystalline forms. The temperature and frequency dependences of the measured ^1H and ^{11}B spin−lattice relaxation rates for the amorphous $Mg(BH_4)_2$ are satisfactorily described in terms of the model with a broad distribution of activation energies centered on $\bar{E}_a = 234$ meV.

Remarkably, the amorphous $Mg(BH_4)_2$ has different reactivity compared to the crystalline forms: we have recently shown that it does not react upon milling with ammonia borane, while the crystalline α- and γ-$Mg(BH_4)_2$ yield a $Mg(BH_4)_2{\cdot}2NH_3BH_3$ complex under the same conditions.[28] So, different reactivity of the amorphous $Mg(BH_4)_2$ thus opens a perspective for creating new reactive hydride composites with improved hydrogen storage properties.

ASSOCIATED CONTENT

Supporting Information

HAADF-STEM images and EDX maps for the amorphous phase; complete references for refs 1, 9, 11, and 16. This material is available free of charge via the Internet at http://pubs.acs.org.

AUTHOR INFORMATION

Corresponding Authors

*(A.V.S.) Fax: +7-343-374-5244; e-mail: skripov@imp.uran.ru.
*(Y.F.) Fax: +32-10-47-27-07; e-mail: yaroslav.filinchuk@uclouvain.be.

Author Contributions

The manuscript was written through contributions of all authors. All authors have given approval to the final version of the manuscript.

Notes

The authors declare no competing financial interest.

ACKNOWLEDGMENTS

This work was partly supported by FNRS (CC 1.5169.12, PDR T.0169.13, EQP U.N038.13), by the Russian Foundation for Basic Research (grant no. 12-03-00078), and by the Priority Program "Physico-technical principles of development of technologies and devices for smart adaptive electrical networks" of the Russian Academy of Sciences. We thank SNBL for the beamtime allocation.

REFERENCES

(1) Ley, M. B.; Jepsen, L. H.; Lee, Y.-S.; Cho, Y. W.; Bellosta von Colbe, J. M.; Dornheim, M.; Rokni, M.; Jensen, J. O.; Sloth, M.; Filinchuk, Y.; et al. Complex Hydrides for Hydrogen Storage − New Perspectives. *Mater. Today* **2014**, *17*, 122−128.

(2) Jepsen, L. H.; Ley, M. B.; Lee, Y.-S.; Cho, Y. W.; Dornheim, M.; Jensen, J. O.; Filinchuk, Y.; Jørgensen, J. E.; Besenbacher, F.; Jensen, T.

R. Boron−Nitrogen Based Hydrides and Reactive Composites for Hydrogen Storage. *Mater. Today* **2014**, *17*, 129−135.
(3) Chong, M.; Karkamkar, A.; Autrey, T.; Orimo, S.-i.; Jalisatgi, S.; Jensen, C. M. Reversible Dehydrogenation of Magnesium Borohydride to Magnesium Triborane in the Solid State under Moderate Conditions. *Chem. Commun.* **2011**, *47*, 1330−1332.
(4) Yu, X. B.; Guo, Y. H.; Sun, D. L.; Yang, Z. X.; Ranjbar, A.; Guo, Z. P.; Liu, H. K.; Dou, S. X. A Combined Hydrogen Storage System of $Mg(BH_4)_2$−$LiNH_2$ with Favorable Dehydrogenation. *J. Phys. Chem. C* **2010**, *114*, 4733−4737.
(5) Filinchuk, Y.; Richter, B.; Jensen, T. R.; Dmitriev, V.; Chernyshov, D.; Hagemann, H. Porous and Dense Magnesium Borohydride Frameworks: Synthesis, Stability, and Reversible Absorption of Guest Species. *Angew. Chem.* **2011**, *123*, 11358−11362.
(6) Černý, R.; Filinchuk, Y.; Hagemann, H.; Yvon, K. Magnesium Borohydride: Synthesis and Crystal Structure. *Angew. Chem., Int. Ed.* **2007**, *46*, 5765−5767.
(7) Her, J.-H.; Stephens, P. W.; Gao, Y.; Soloveichik, G. L.; Rijssenbeek, J.; Andrus, M.; Zhao, J.-C. Structure of Unsolvated Magnesium Morohydride $Mg(BH_4)_2$. *Acta Crystallogr., Sect. B: Struct. Sci.* **2007**, *63*, 561−568.
(8) Ban, V.; Černý, R.; Richter, B.; Jensen, T. R.; Webb, C. J.; Morelle, F.; Filinchuk, Y. **2014**, submitted for publication.
(9) David, W. I. F.; Callear, S. K.; Jones, M. O.; Aeberhard, P. C.; Culligan, S. D.; Pohl, A. H.; Johnson, S. R.; Ryan, K. R.; Parker, J. E.; Edwards, P. P.; et al. The Structure, Thermal Properties and Phase Transformations of the Cubic Polymorph of Magnesium Tetrahydroborate. *Phys. Chem. Chem. Phys.* **2012**, *14*, 11800−11807.
(10) Paskevicius, M.; Pitt, M. P.; Webb, C. J.; Sheppard, D. A.; Filsø, U.; Gray, E. M.; Buckley, C. E. In-Situ X-ray Diffraction Study of γ-$Mg(BH_4)_2$ Decomposition. *J. Phys. Chem. C* **2012**, *116*, 15231−15240.
(11) Rude, L. H.; Nielsen, T. K.; Ravnsbæk, D. B.; Bösenberg, U.; Ley, M. B.; Richter, B.; Arnbjerg, L. M.; Dornheim, M.; Filinchuk, Y.; Besenbacher, F.; et al. Tailoring Properties of Borohydrides for Hydrogen Storage: A Review. *Phys. Status Solidi A* **2011**, *208*, 1754−1773.
(12) Hwang, S.-J.; Bowman, R. C.; Reiter, J. W.; Rijssenbeek, J.; Soloveichik, G. L.; Zhao, J.-C.; Kabbour, H.; Ahn, C. C. NMR Confirmation for Formation of $[B_{12}H_{12}]^{2-}$ Complexes during Hydrogen Desorption from Metal Borohydrides. *J. Phys. Chem. C* **2008**, *112*, 3164−3169.
(13) Zhao-Karger, Z.; Witter, R.; Bardaji, E. G.; Wang, D.; Cossement, D.; Fichtner, M. Altered Reaction Pathways of Eutectic $LiBH_4$-$Mg(BH_4)_2$ by Nanoconfinement. *J. Mater. Chem. A* **2013**, *1*, 3379−3386.
(14) Ravnsbæk, D. B.; Filinchuk, Y.; Černý, R.; Jensen, T. R. Powder Diffraction Methods for Studies of Borohydride-Based Energy Storage Materials. *Z. Kristallogr.* **2010**, *225*, 557−569.
(15) Bardají, E. G.; Hanada, N.; Zabara, O.; Fichtner, M. Effect of Several Metal Chlorides on the Thermal Decomposition Behaviour of α-$Mg(BH_4)_2$. *Int. J. Hydrogen Energy* **2011**, *36*, 12313−12318.
(16) Pistidda, C.; Garroni, S.; Dolci, F.; Bardají, E. G.; Khandelwal, A.; Nolis, P.; Dornheim, M.; Gosalawit, R.; Jensen, T.; Cerenius, Y.; et al. Synthesis of Amorphous $Mg(BH_4)_2$ from MgB_2 and H_2 at Room Temperature. *J. Alloys Compd.* **2010**, *508*, 212−215.
(17) Eagles, M.; Sun, B.; Richter, B.; Jensen, T. R.; Filinchuk, Y.; Conradi, M. S. NMR Investigation of Nanoporous γ-$Mg(BH_4)_2$ and Its Thermally Induced Phase Changes. *J. Phys. Chem. C* **2012**, *116*, 13033−13037.
(18) Cui, S.; Liao, S.; Zhang, Y.; Xu, Y.; Miao, Y.; Lu, M.; Fan, Y.; Guo, W. Synthesis of Nanometric-Size Magnesium Nitride by the Nitriding of Pre-activated Magnesium Powder. *J. Mater. Sci.* **1999**, *34*, 5601−5604.
(19) Radha, A. V.; Forbes, T. Z.; Killian, C. E.; Gilbert, P. U. P. A.; Navrotsky, A. Transformation and Crystallization Energetics of Synthetic and Biogenic Amorphous Calcium Carbonate. *Proc. Natl. Acad. Sci. U.S.A.* **2010**, *107*, 16438−16443.
(20) Filinchuk, Y.; Černý, R.; Hagemann, H. Insight into $Mg(BH_4)_2$ with Synchrotron X-ray Diffraction: Structure Revision, Crystal Chemistry, and Anomalous Thermal Expansion. *Chem. Mater.* **2009**, *21*, 925−933.
(21) Abragam, A. *The Principles of Nuclear Magnetism*; Clarendon Press: Oxford, U.K., 1961.
(22) Soloninin, A. V.; Babanova, O. A.; Skripov, A. V.; Hagemann, H.; Richter, B.; Jensen, T. R.; Filinchuk, Y. NMR Study of Reorientational Motion in Alkaline-Earth Borohydrides: β and γ Phases of $Mg(BH_4)_2$ and α and β Phases of $Ca(BH_4)_2$. *J. Phys. Chem. C* **2012**, *116*, 4913−4920.
(23) Shane, D. T.; Rayhel, L. H.; Huang, Z.; Zhao, J.-C.; Tang, X.; Stavila, V.; Conradi, M. S. Comprehensive NMR Study of Magnesium Borohydride. *J. Phys. Chem. C* **2011**, *115*, 3172−3177.
(24) Skripov, A. V.; Soloninin, A. V.; Babanova, O. A.; Hagemann, H.; Filinchuk, Y. Nuclear Magnetic Resonance Study of Reorientational Motion in α-$Mg(BH_4)_2$. *J. Phys. Chem. C* **2010**, *114*, 12370−12374.
(25) Markert, J. T.; Cotts, E. J.; Cotts, R. M. Hydrogen Diffusion in the Metallic Glass a-$Zr_3RhH_{3.5}$. *Phys. Rev. B* **1988**, *37*, 6446−6452.
(26) Skripov, A. V.; Soloninin, A. V.; Ley, M. B.; Jensen, T. R.; Filinchuk, Y. Nuclear Magnetic Resonance Studies of BH_4 Reorientations and Li Diffusion in $LiLa(BH_4)_3Cl$. *J. Phys. Chem. C* **2013**, *117*, 14965−14972.
(27) Chapman, K. W.; Halder, G. J.; Chupas, P. J. Pressure-Induced Amorphization and Porosity Modification in a Metal−Organic Framework. *J. Am. Chem. Soc.* **2009**, *131*, 17546−17547.
(28) Jepsen, L. H.; Ban, V.; Møller, K. T.; Lee, Y.-S.; Cho, Y. W.; Besenbacher, F.; Filinchuk, Y.; Skibsted, J.; Jensen, T. R. Synthesis, Crystal Structure, Thermal Decomposition, and ^{11}B MAS NMR Characterization of $Mg(BH_4)_2(NH_3BH_3)_2$. *J. Phys. Chem. C* **2014**, *118*, 12141−12153.